RSC Advances

This is an *Accepted Manuscript*, which has been through the Royal Society of Chemistry peer review process and has been accepted for publication.

Accepted Manuscripts are published online shortly after acceptance, before technical editing, formatting and proof reading. Using this free service, authors can make their results available to the community, in citable form, before we publish the edited article. This *Accepted Manuscript* will be replaced by the edited, formatted and paginated article as soon as this is available.

You can find more information about *Accepted Manuscripts* in the Information for Authors.

Please note that technical editing may introduce minor changes to the text and/or graphics, which may alter content. The journal's standard Terms & Conditions and the Ethical guidelines still apply. In no event shall the Royal Society of Chemistry be held responsible for any errors or omissions in this *Accepted Manuscript* or any consequences arising from the use of any information it contains.

ROYAL SOCIETY OF CHEMISTRY

www.rsc.org/advances

Controlled synthesis of the $Zn_{(1-1.5x)}Fe_xS$ nanoparticles via microwave route and their photocatalytic properties

Weijie Zhao [a], Jing Zhang *[a], Guangshan Zhang *[b], Limin Xi [a], Hangui Wu [a] and Zhikui Hao [a]

[a]*School of Biological and Chemical Engineering, Taizhou Vocational & Technical College, Taizhou 318000, PR China*

[b]*School of Municipal and Environmental Engineering, Harbin Institute of Technology, Harbin 150090, PR China*

*Corresponding authors. Tel.: 86-576-88663356; Fax: 86-576-88663356.

E-mail address: zwjzj2000@126.com (Jing Zhang), gszhanghit@gmail.com (G.S. Zhang)

RSC Advances Accepted Manuscript

Abstract

Fe-doped ZnS photocatalysts synthesized by a conventional hydrothermal method usually had poor crystallity and low photocatalytic activity. In this study, the $Zn_{(1-1.5x)}Fe_xS$ particles were first directly synthesized by the microwave irradiation method without additional heat treatments. The prepared $Zn_{(1-1.5x)}Fe_xS$ catalysts were characterized using X-ray diffraction (XRD), UV-Vis Absorption Spectra, scanning electron microscopy (SEM), and Brunauer-Emmett-Teller (BET) analyzer, etc. The characterization results show that the morphology and physico-chemical properties of samples are changed depending on the ration of Fe and Zn. The absorption edges of $Zn_{(1-1.5x)}Fe_xS$ were red-shifted as the value of x decreased. The band gaps were estimated to be from 2.74 to 3.64 eV from the onset of the UV-Vis absorption edges. The results indicated that the photocatalyst of $Zn_{0.97}Fe_{0.02}S$ has the highest photocatalytic activity of Dimethyl phthalate (DMP) with the removal of 97.5%. In addition, the crystallite size, band gap and structure for the $Zn_{(1-1.5x)}Fe_xS$ samples have a strong influence on the degradation of DMP from wastewater.

Keywords: dimethyl phthalate; microwave; photocatalyst; $Zn_{(1-1.5x)}Fe_xS$

RSC Advances Accepted Manuscript

1. Introduction

DMP is one of the most important endocrine disruptors which are a major class of environmental contaminants and widely used as plasticizers to improve the flexibilityand durability of consumer products, food packaging materials, and polyvinyl chloride plastics.[1, 2] Nowadays, DMP are suspected to be mutagens, endocrine disruptors and hepatotoxic agents, and can accumulate in human body, and might pose a risk to human health.[3, 4] Due to their widespread presence, persistence, and difficulty in degradation, the United States Environmental Protection Agency has listed DMP as the priority pollutant.[5, 6] As a result, different treatment methods for DMP-contaminated water have attracted research attention.

Over the past decades, various chemical, physical and biological techniques, for the removal of DMP have been developed, including advanced oxidation processes, constructed wetlands, anaerobicdegradation, microwave and photocatalysis.[1, 6-9] Recently, a great deal of attention has been paid to the photodegradation of DMP by inorganic materials, especially ZnS-based semiconductors.[10-12] There are many preparation methods for Fe-doped ZnS, such as hydrothermal,[13, 14] microemulsion,[15] and chemical co-precipitation method.[16-19] Contrasted with the above-mentioned methods, microwave irradiation method is a environmentally friendly and economical method to synthesize materials,[20, 21] probably due to its outstanding advantages of fast reaction speed and clean reaction way.[22, 23] Consequently, some photocatalytic materials such as β-Ga_2O_3[24] and ZnS[21] have been synthesized using microwave method instead of the conventional methods.

In the study, Fe-doped ZnS materials with different Fe concentration were synthesized through microwave irradiation. The physical properties, crystal structure and photocatalytic performance of the prepared nanoparticles were manipulated.

RSC Advances Accepted Manuscript

Particularly, we analyze the photocatalyst band structures under different *x* values according to characterization results and experimental data.

2. Experimental

2.1. Chemicals

The starting materials for the synthesis of $Zn_{(1-1.5x)}Fe_xS$ nanoparticles were $Zn(NO_3)_2 \cdot 6H_2O$ and $Fe(NO_3)_3 \cdot 9H_2O$ as zinc and iron sources, respectively. Thioacetamide (TAA) was applied as a sulfur source, and 2-Mercaptoethanol (2-hydroxyethanthiol, $HOCH_2CH_2SH$) was applied as a stabilizing agent. All chemicals were of the highest purity available and used without further purification. All solutions were prepared using deionized (DI) water at room temperature.

2.2. Synthesis

Microwave irradiation hydrothermal synthesis procedure was as follows. Briefly, appropriate amounts of $Zn(NO_3)_2 \cdot 6H_2O$ and $Fe(NO_3)_3 \cdot 9H_2O$ (totaling to 10 mmol) were dissolved in 100 mL of deionized (DI) water using a mechanical stirrer, in which specific amounts of the two compounds were calculated in Table S1 in supporting information. And then 10 mmol of TAA and 1.0 mL of 2-Mercaptoethanol were into the above-mentioned solution, stirring and obtaining a mixture. The flask was moved into the Microwave reactor (COOLPEX-E with output power 1200 W, purchased from PreeKem Scientific Instruments Co., Ltd., China). Fig. 1 shows the picture of the Microwave reactor. As the volume of the mixed solution was less than 100 mL, all experiments were conducted at P_{MW} = 500 W according to the instruction of MW reactor. The reaction was carried out at 388 K for 30 min in the MW reactor with a reflux condenser and a mechanical stirrer. After it was finished, the mixture was cooled till room temperature. The precipitated nanoparticles were separated in a centrifuge (at 7000 rpm) within 15 min, and washed by distillated water and absolute

RSC Advances Accepted Manuscript

ethyl alcohol rigorously. Finally, the mixture was vacuum dried at 358 K for 60 min. The photocatalysts were further characterized using methods as described in following section.

2.3. Characterization

XRD analysis was conducted on a Philips X'pert diffractometer equipped with an X'celerator module using Cu Kαradiation. Diffractograms were obtained for 2θ= 10-70° with a step size of 0.0167°.

UV-Vis absorption spectrum of the photocatalyst was measured using an absorption spectrophotometer (Bechman, DU7000). The spectral region was from 200 to 800 nm operating at a resolution of 2 nm. The sample cell was a quartz cuvette (1 cm by 1 cm).

The metallic elemental composition of the photocatalyst was measured with a Perkin Elmer Optima NexIon^{TM} 300 ICP-MS (Inductively Coupled Plasma Mass Spectrometry) system. Briefly, 50 mg of the powder catalyst were digested by adding 2 mL HNO_3 (67–70%, v/v) and 1 mL H_2O_2 (30 wt% in H_2O). Then the suspension washeated on a hotplate at 150°C for 20 min with a watch glass covering the beaker. The S composition of the photocatalyst was analyzed by Ion Chromatography (IC) on a Dionex AS50 equipped with an ED50 electrochemical detector and an AS9-HC column. The mobile phase was a solution of 9 mM Na_2CO_3, and the flow rate was set at 1.0 mL·min^{-1}.

The Brunauer-Emmett-Teller (BET) surface area was determined by the N_2 physisorption measurement performed on a Micromeritics ASAP 2020 physisorption analyzer. Prior to analysis, samples were degassed at 200°C for 4 h under vacuum. The BET surface area was calculated from the adsorption isotherm in the region 0.05 $< P/P_0 <$ 0.3.

RSC Advances Accepted Manuscript

SEM images were obtained on a Zeiss Ultra60 microscope with an accelerating voltage of 20 kV. The sample powder was spread on a carbon-coated sample mount and coated with gold to prevent surface charging effects. Optimum images were taken using the "inlens" detector mode and 5.5 mm of working distance. Elemental analysis of the powder catalyst was performed using EDS with the Zeiss Ultra60 FE-SEM.

The morphology of the sample was determined by TEM on an FEI-Tecnai F20 FEG-TEM with an accelerating voltage of up to 200 kV. TEM samples were prepared by placing 5 μL of the aqueous $Zn_{(1-1.5x)}Fe_xS$ water suspension on copper grids with a continuous carbon film coating, followed by solvent evaporation at room temperature.

2.4. Photocatalytic activities of $Zn_{(1-1.5x)}Fe_xS$ nanoparticles

Photocatalytic removal experiments were conducted in a cylindrical reactor (Fig. 2). In the experiment, the solution was made by adding 0.1 g of $Zn_{(1-1.5x)}Fe_xS$ powder to 300 mL aqueous solution of DMP with a concentration of 10 mg/L at pH 6.5. The pH value of the initial reaction solution was adjusted by adding 0.1 M HCl or 0.1 M NaOH solutions. Before irradiation, the suspension was magnetically stirred in the darkfor 30 min to ensure adsorption equilibrium of DMP on the catalysts. Simulated solar light (SSL) irradiation was provided by a 500-W xenon lamp (dominant wavelength is 250 nm-1000 nm) that was positioned in the cylindrical quartz cold trap. The irradiation intensity was about 1.2 W cm^{-2} measured by a FZ-A spectroradiometer (the photoelectric instrument factory of Beijing Normal University, China). The system was cooled by circulating water and maintained at room temperature (20 ^{o}C). Approximately 3.0 mL of reaction solution was taken at given time intervalsand centrifuged to separate the catalyst powder for DMP analysis.

DMP concentrationwas analyzed by HPLC instrument (LC-20AD; SHIMADZU) equipped with an electrolytic conductivity detector (CDD-10AVP;SHIMADZU). Mobile phase A was methanol and phase B was the DI water containing 20 mmol/L

RSC Advances Accepted Manuscript

of KH_2PO_4, and flow rate was0.8 mL/min. The limit of detection for DMA is 0.01 mg/L inthis experiment. All measurements of the DMP degradation at different irradiation times were performed three times to confirm their reproducibility. The presented data points are mean values with SDs as error bars. The removal efficiency of DMP can be calculated by :

$$R = \frac{C_0 - C}{C_0} \times 100\% \quad (1)$$

where R, C_0 and C arethe removal efficiency of DMP, initial concentration of solution and concentration of DMP after irradiation at various time interval (t), respectively.

3. Results and discussion

3.1. X-ray diffraction and specific surface areasof $Zn_{(1-1.5x)}Fe_xS$

The XRD patterns were used for characterization and evaluated of crystallite sizes of the synthesized $Zn_{(1-1.5x)}Fe_xS$. Fig. 3 shows the XRD patterns of $Zn_{(1-1.5x)}Fe_xS$(x = 0, 0.006, 0.01, 0.02 and 0.03). Despite the different x values, the XRD patternsof these photocatalysts are similar, which indicates thatthe x value had a negligible effect on the crystallinity.Three major peaks are clearly observed at 2θ values of 28.5º, 47º, and 55.5º with indexed as (111), (200), and (222), which they well correspond to the standard card JCPDS No. 5-566.[25, 26] The Fe metal peaks were not observed in the XRD patterns of all obtained $Zn_{(1-1.5x)}Fe_xS$, indicating the added Fe ions should entered into ZnS host lattice as substituent.[13]

With the decreasing Fe content in the $Zn_{(1-1.5x)}Fe_xS$, the diffraction peaks gradually shift toward the smaller angle, which agrees with previous findings.[16] The successive shift of XRD patterns also implies that crystals of the $Zn_{(1-1.5x)}Fe_xS$ photocatalyst were not a simple physical mixture of FeS and ZnS.

The crystallite size was determined using the Scherrer equation:[27, 28]

RSC Advances Accepted Manuscript

$$D = \frac{0.9\lambda}{B\cos\theta} \quad (2)$$

where D is the crystallite size (nm), λ is the wavelength of the incident X-ray (0.15406 nm), θ is the diffraction angle of the (111) peak plane (degree), and B corresponds to the full width at half-maximum of the crystalline plane (radian). The size of $Zn_{(1-1.5x)}Fe_xS$ particles was calculated accordance to the Scherrer equation and shown in Table 1. The crystallite sizes of all obtained samples were from 48.2 to 65.5 nm.

The calculated BET surface areas of $Zn_{(1-1.5x)}Fe_xS$ were also listed in Table 1. The highest BET surface area of 85.7 m^2 $g^{-1}$was found in ZnS (x = 0). Introducing Fe^{3+} into the lattice ZnS resulted in a significant decrease of BET surface areas, possibly owing to particle agglomeration upon the microwave synthesis process, the blocking of the greater accumulation of Fe on ZnS surface.[16]

3.2. Elemental analysis of $Zn_{(1-1.5x)}Fe_xS$

The chemical compositions of the catalysts determined with ICP-MS and IC are shown in Table 2. The measured element compositions closely match the theoretical formula of $Zn_{(1-1.5x)}Fe_xS$, particularly for the catalyst that was synthesized at x = 0.02. Fig. 4 shows the EDS analysis result that also indicates the presence of chemical elemental Zn, Fe, and S in the $Zn_{0.97}Fe_{0.02}S$ catalyst. It is clear that Fe ions have been incorporated in Zn^{2+} lattice sites.

3.3. UV-vis absorption spectra of $Zn_{(1-1.5x)}Fe_xS$

Fig. 5(a) shows the UV-Vis absorption spectra of as-prepared $Zn_{(1-1.5x)}Fe_xS$ photocatalysts. ZnS had no light absorption in visible-light region, whereas the absorption edge for the $Zn_{(1-1.5x)}Fe_xS$ ($0 < x \leq 0.03$) samples is red-shifted relative to ZnS, which is attributed to the incorporation of Fe into the lattice of ZnS. These $Zn_{(1-1.5x)}Fe_xS$ ($x \geq 0.01$) photocatalysts had intense absorption bands with steep edges

RSC Advances Accepted Manuscript

196 in the visible light region, indicating that the visible-light absorption was due to a
197 band gap transition rather than to the transition of impurity energies to the CB of
198 $Zn_{(1-1.5x)}Fe_xS$; this phenomenon was also observed for metal-ion-doped ZnS
199 photocatalysts.[29, 30]

200 According to the Kubelka-Munk function, the band gaps of the $Zn_{(1-1.5x)}Fe_xS$
201 samplescan be determined from the plot of $(\alpha hv)^2$ versus theenergy of the excitation
202 light (hv), where α is the absorption coefficient (the absorbance in Fig. 5(a)) and hv is
203 the incident photon energy.[31, 32] The plots of $(\alpha hv)^2$ versus hv for the $Zn_{(1-1.5x)}Fe_xS$
204 samples are shown in Fig. 5(b). Extrapolation of linear regions of the plots to zero
205 value can give the direct band gap values, which are listed in Table 1. These samples
206 have optical absorption gaps of 3.64 eV, 3.28 eV, 2.96 eV, 2.85 eV and 2.74 eV for
207 ZnS, $Zn_{0.991}Fe_{0.006}S$, $Zn_{0.985}Fe_{0.01}S$, $Zn_{0.97}Fe_{0.02}S$ and $Zn_{0.955}Fe_{0.03}S$, respectively. The
208 decreasing band gap suggests that incorporating Fe ions in ZnS can effectively reduce
209 its band gap into the visible light absorption region.

210 3.4. Morphology of $Zn_{(1-1.5x)}Fe_xS$

211 TEM and SEM images were performed to assess the size, morphology and
212 microstructure of the nanoparticles. The SEM and TEM micrographs of the
213 $Zn_{0.97}Fe_{0.02}S$ (x = 2) photocatalystwere shown in Fig. 6. Fig. 6(a) shows that the
214 agglomerates of particles and not the crystallite size. It was not possible by SEM
215 image to calculate the crystallite size due to the resolution limit. Although the
216 particles were aggregated, it is clear that the particle morphology is cubic. The more
217 precise size distribution of nanocrystallites was performed by TEM. As shown in Fig.
218 6(b), the average particle size of the $Zn_{0.97}Fe_{0.02}S$ photocatalysts based on the
219 statistical measurement (no less than 30 particles were counted) was 50 nm, which
220 agrees well with the crystallite size derived from the XRD results.

RSC Advances Accepted Manuscript

3.5. Calculation of band edge levels of $Zn_{(1-1.5x)}Fe_xS$

The positions of conduction band and valence band of the $Zn_{(1-1.5x)}Fe_xS$ samples in relation to the normal hydrogen electrode (NHE) potential can be calculated using the following equations.[33-35]

$$E_{CB} = X - E_0 - \frac{1}{2}E_g \quad (3)$$

$$X = \left\{ x_{Zn}^{1-1.5x} \times x_{Fe}^{x} \times x_{S}^{1} \right\}^{1/(2-0.5x)} \quad (4)$$

$$X_{Zn} = \frac{1}{2}(A_{Zn} + I_{Zn}) \quad (5)$$

$$X_{Fe} = \frac{1}{2}(A_{Fe} + I_{Fe}) \quad (6)$$

$$x = \frac{1}{2}(A + I) \quad (7)$$

where X is the absolute electronegativity of a pristine semiconductor and is expressed as the geometric mean of x of the constituent atoms; x is the electronegativity of a neutral atom; E_0 is the energy of a free electron on the hydrogen scale (~4.5 eV); E_g is the semiconductor band gap energy (eV); A is the atom's electron affinity; I is the first ionization energy. The data of A and I obtained from Ref.[36]

Using Eqs. (3)-(7), the band positions for E_{CB}, and E_{VB} can be calculated in shown Tables 3 and 4. It should be noted that the band edges calculated are approximate. The E_{CB} becomes more negative with decreasing x value in the $Zn_{(1-1.5x)}Fe_xS$ samples, indicating that the Zn-doped sulfide has stronger oxidation activity for DMP removal than those sulfides doped with Fe. However, ZnS itself has a large band gap (3.64 eV) and thus cannot utilize visible light for DMP removal. Thus, the best photocatalytic activity should be achieved by keeping the balance between the oxidation power and light absorption.[37]

RSC Advances Accepted Manuscript

3.6. Photocatalytic response of $Zn_{(1-1.5x)}Fe_xS$ nanoparticles

Fig. 7 shows the removal efficiency of DMP under visible light in the presence of undoped and Fe-doped ZnS under visible light (inset shows its ln C_0/C vs. time graph). No DMP was removed without the $Zn_{(1-1.5x)}Fe_xS$ photocatalysts under Xe lamp irradiation. As shown in Fig. 7(a), the removal efficiency of DMP increased gradually with x value from 0 and reached a maximum level (97.5%) at x = 0.02. According to the calculation results, the $Zn_{0.97}Fe_{0.02}S$ had the highest crystallinity and the highest specific surface area, which explained its high photocatalytic activity. Further increase in x value from 0.02 to 0.03 decreased the removal efficiency of DMP, probably because of the decreased specific surface area and low crystallinity structure. Here, many crystal defects on $Zn_{0.955}Fe_{0.03}S$ appeared , which may serve as recombination centers to decrease the degradation efficiency. Moreover, the removal efficiency of DMP using ZnS (x =0) was only 18% that of the $Zn_{0.97}Fe_{0.02}S$ (x = 0.02), indicating that the ratio of Fe and Zn is critical for improving the photocatalyst activity.

Fig. 7(b) shows that the photocatalytic degradation of DMP followed the first-order decay kinetics. The experimental data indicate that the photocatalytic degradation of DMP can be described by the first-order kinetic model, $\ln(C_0/C) = kt$, where C_0 and C are initial concentration of solution, concentration of DMP after irradiation at various time interval (t), respectively. The $\ln(C_0/C)$ vs. t plot shows a linear relation ship with the irradiation time. The calculated rate constant (k) for ZnS was 1.4×10^{-3} min^{-1} and the k values of $Zn_{0.991}Fe_{0.006}S$, $Zn_{0.985}Fe_{0.01}S$, $Zn_{0.97}Fe_{0.02}S$ and $Zn_{0.955}Fe_{0.03}S$ were 7.0 $\times 10^{-3}$, 1.9×10^{-2}, 2.9×10^{-3}, and 2.1×10^{-3} min^{-1}, respectively. It is clear that the doping of Fe in ZnS can increase the photocatalytic degradation of DMP under the visible light. In the meanwhile, the photocatalytic activity of Fe doped ZnS is strongly dependent on the dopant concentration.

RSC Advances Accepted Manuscript

4. Conclusions

In conclusion, $Zn_{(1-1.5x)}Fe_xS$ synthesized by the microwave irradiation method is found to be high active for the DMP removal. In the synthesized method, the reation time under microwave irradiation was only 30 min at 388 K and the vacuum drying time was only 60 min at 358 K, and the subsequent procedure did not need the calcination. The crystallite size, BET specific surface area, band gaps and band edge positions of the photocatalysts could be controlled by adjusting the atomic ratios of the Zn and Fe components. The photocatalyst of $Zn_{0.97}Fe_{0.02}S$ has the best photocatalytic activity to remove DMP from wastewater. This work not only provides a facile and friendly synthesized method to produce highly active $Zn_{(1-1.5x)}Fe_xS$ materials for removing DMP from water or wastewater, but also demonstrates new insights into understanding the photocatalytic activity through controlling synthesis process.

Acknowledgments

The work was supported by the Program of Marine Biological Resources Exploitation and Utilization of Science and Technology Innovation Team of Taizhou (Document of CPC Taizhou Municipal Committee Office of Zhejiang Province NO. [2012]58), School of Biological and Chemical Engineering, Taizhou Vocational & Technical College.This work was also supported by the National Natural Science Foundation of China (No.21301155) and Zhejiang Provincial Natural Science Foundation of China (LY13E020012).

RSC Advances Accepted Manuscript

Notes and references

1 X. Y. Tang, S. Y. Wang, Y. Yang, R. Tao, Y. Dai, A. Dan and L. Li, *Chemical Engineering Journal*, 2015, **275**, 198-205.

2 M. A. Surhio, F. N. Talpur, S. M. Nizamani, F. Amin, C. W. Bong, C. W. Lee, M. A. Ashraf and M. R. Shah, *Rsc Advances*, 2014, **4**, 55960-55966.

3 Z. W. Xu, W. M. Zhang, L. Lv, B. C. Pan, P. Lan and Q. X. Zhang, *Environmental Science & Technology*, 2010, **44**, 3130-3135.

4 L. J. Xu, W. Chu and L. Gan, *Chemical Engineering Journal*, 2015, **263**, 435-443.

5 B. Xu, N. Y. Gao, H. F. Cheng, S. J. Xia, M. Rui and D. D. Zhao, *Journal of Hazardous Materials*, 2009, **162**, 954-959.

6 B. L. Yuan, X. Z. Li and N. Graham, *Water Research*, 2008, **42**, 1413-1420.

7 Y. Wang, Y. Liu, T. Liu, S. Song, X. Gui, H. Liu and P. Tsiakaras, *Applied Catalysis B: Environmental*, 2014, **156**, 1-7.

8 D. Han, J. Li, H. Cao, M. He, J. Hu and S. Yao, *Chemosphere*, 2014, **95**, 50-57.

9 D. W. Liang, T. Zhang and H. H. P. Fang, *Water Research*, 2007, **41**, 2879-2884.

10 Y. H. Chen, N. C. Shang, L. L. Chen, C. Y. Chang, P. C. Chiang, C. Y. Hu and C. H. Chang, *Desalination and Water Treatment*, 2014, **52**, 3377-3383.

11 Z. J. Huang, P. X. Wu, Y. H. Lu, X. R. Wang, N. W. Zhu and Z. Dang, *Journal of Hazardous Materials*, 2013, **246**, 70-78.

12 W. C. Liao, T. Zheng, P. Wang, S. S. Tu and W. Q. Pan, *Environmental Engineering Science*, 2010, **27**, 1001-1007.

13 N. Wetchakun, B. Incessungvorn, K. Wetchakun and S. Phanichphant, *Materials Research Bulletin*, 2013, **48**, 1668-1674.

14 S. Kumar and N. K. Verma, *Journal of Materials Science: Materials in Electronics*, 2015, **26**, 2754-2759.

15 Y. Li, C. Cao and Z. Chen, *Chemical Physics Letters*, 2011, **517**, 55-58.

16 P. C. Patel and P. C. Srivastava, *Journal of Materials Science*, 2014, **49**, 6012-6019.

17 S. Sambasivam, D. P. Joseph, D. R. Reddy, B. K. Reddy and C. K. Jayasankar, *Materials Science and Engineering B: Advanced Functional Solid-State Materials*, 2008, **150**, 125-129.

18 R. Chauhan, A. Kumar and R. P. Chaudhary, *Spectrochimica Acta Part A: Molecular and Biomolecular Spectroscopy*, 2013, **113**, 250-256.

19 R. Chauhan, A. Kumar and R. P. Chaudhary, *Applied Surface Science*, 2013, **270**, 655-660.

RSC Advances Accepted Manuscript

20 W. C. Liao and P. Wang, *Journal of the Brazilian Chemical Society*, 2009, **20**, 866-872.
21 L. X. Yin, D. Wang, H. J. Feng, L. Y. Cao, H. B. Ouyang, J. P. Wu and X. Yong, *Ceramics International*, 2015, **41**, 3288-3292.
22 T. Prakash, G. Neri, A. Bonavita, E. R. Kumar and K. Gnanamoorthi, *Journal of Materials Science: Materials in Electronics*, 2015, **26**, 4913-4921.
23 K. Vijayalakshmi and S. D. Jereil, *Journal of Materials Science: Materials in Electronics*, 2014, **25**, 5089-5094.
24 B. X. Zhao, X. Li, L. Yang, F. Wang, J. C. Li, W. X. Xia, W. J. Li, L. Zhou and C. l. Zhao, *Photochemistry and photobiology*, 2015, **91**, 42-47.
25 H. R. Rajabi, O. Khani, M. Shamsipur and V. Vatanpour, *Journal of Hazardous Materials*, 2013, **250–251**, 370-378.
26 O. Khani, H. R. Rajabi, M. H. Yousefi, A. A. Khosravi, M. Jannesari and M. Shamsipur, *Spectrochimica Acta Part A: Molecular and Biomolecular Spectroscopy*, 2011, **79**, 361-369.
27 D. H. Wang, L. Wang and A. W. Xu, *Nanoscale*, 2012, **4**, 2046-2053.
28 G. S. Zhang, W. Zhang, D. Minakata, Y. S. Chen, J. Crittenden and P. Wang, *International Journal of Hydrogen Energy*, 2013, **38**, 11727-11736.
29 G. S. Zhang, W. Zhang, D. Minakata, P. Wang, Y. S. Chen and J. Crittenden, *International Journal of Energy Research*, 2014, **38**, 1513-1521.
30 Q. Li, H. Meng, P. Zhou, Y. Q. Zheng, J. Wang, J. G. Yu and J. R. Gong, *ACS Catalysis*, 2013, **3**, 882-889.
31 K. Li, B. Chai, T. Peng, J. Mao and L. Zan, *Rsc Advances*, 2013, **3**, 253-258.
32 E. S. Agorku, M. A. Mamo, B. B. Mamba, A. C. Pandey and A. K. Mishra, *Journal of Porous Materials*, 2015, **22**, 47-56.
33 M. A. Butler and D. S. Ginley, *Journal of the Electrochemical Society*, 1978, **125**, 228-232.
34 Y. Xu and M. A. A. Schoonen, *American Mineralogist*, 2000, **85**, 543-556.
35 G. S. Zhang, W. Zhang, J. C. Crittenden, Y. S. Chen, D. Minakata and P. Wang, *Chinese Journal of Catalysis*, 2013, **34**, 1926-1935.
36 D. R. Lida, *Handbook of Chemistry and Physics*, CRC Press, Florida, 87th edn., 2006-2007.
37 S. H. Mohamed, *Journal of Physics D: Applied Physics*, 2010, **43**, 035406.

RSC Advances Accepted Manuscript

RSC Advances Accepted Manuscript

367 **Table 1**

368 Characterization results of $Zn_{(1-1.5x)}Fe_xS$ ($0 \leq x \leq 0.03$) photocatalysts.

Value of x	Crystallite size (nm)	Surface area ($m^2\ g^{-1}$)	Band gap (eV)	Absorption edge (nm)
0	65.5	85.7	3.64	341
0.006	56.4	61.8	3.28	378
0.01	49.7	68.9	2.96	419
0.02	48.2	75.6	2.85	435
0.03	48.5	73.8	2.74	453

RSC Advances Accepted Manuscript

369 **Table 2**

370 Element compositions of the catalysts synthesized at different *x* values.

Value of *x*	Chemical formula
0	$Zn_{(0.995\pm0.002)}S$
0.006	$Zn_{(0.990\pm0.005)}Fe_{(0.006\pm0.001)}S$
0.01	$Zn_{(0.985\pm0.004)}Fe_{(0.01\pm0.002)}S$
0.02	$Zn_{(0.970\pm0.003)}Fe_{(0.02\pm0.001)}S$
0.03	$Zn_{(0.956\pm0.004)}Fe_{(0.03\pm0.002)}S$

RSC Advances Accepted Manuscript

371 **Table 3**

372 Values of the electron affinity, ionization energy and element electronegativity.

Constituent elements	Electron affinity (eV)	Ionization energy (eV)	Element electronegativity (eV)
Fe	0.151	7.902	4.026
Zn	-0.87	9.394	4.262
S	2.077	10.36	6.2182

RSC Advances Accepted Manuscript

373 **Table 4**

374 X, E_g, E_{CB}, and E_{VB} at the point of zero charge for $Zn_{(1-1.5x)}Fe_xS$.

Value of x	X (eV)	E_g (eV)	E_{CB} (eV)	E_{VB} (eV)
0	5.148	3.64	-1.17	2.47
0.006	5.149	3.28	-0.99	2.29
0.01	5.149	2.96	-0.83	2.13
0.02	5.150	2.85	-0.78	2.08
0.03	5.151	2.74	-0.72	2.02

RSC Advances Accepted Manuscript

Fig. 1 The picture of the Microwave reactor.

RSC Advances Accepted Manuscript

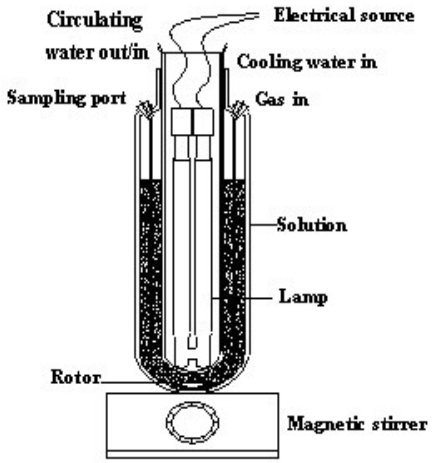

377

378 Fig. 2 Schematic diagram of photochemical reaction device.

RSC Advances Accepted Manuscript

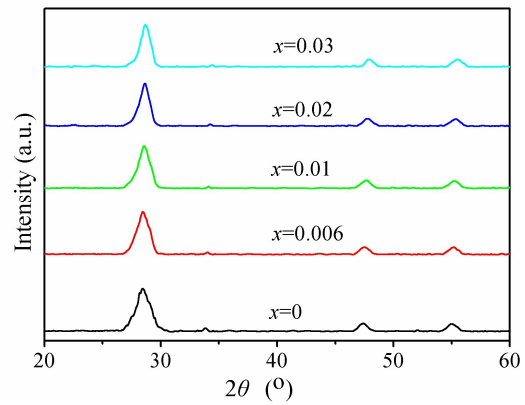

Fig. 3 XRD patterns of undoped and Fe doped (x = 0.006, 0.01, 0.02 and 0.03) ZnS nanoparticles.

RSC Advances Accepted Manuscript

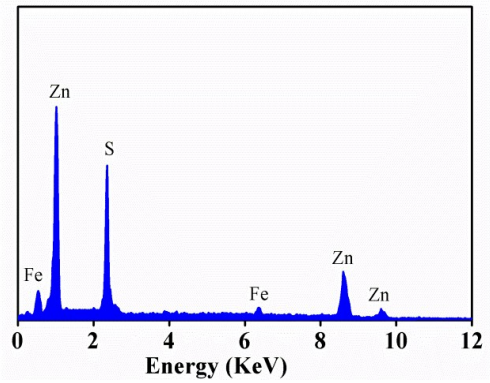

Fig. 4 Energy-dispersive X-ray spectroscopy spectrum of the $Zn_{0.97}Fe_{0.02}S$ photocatalysts.

RSC Advances Accepted Manuscript

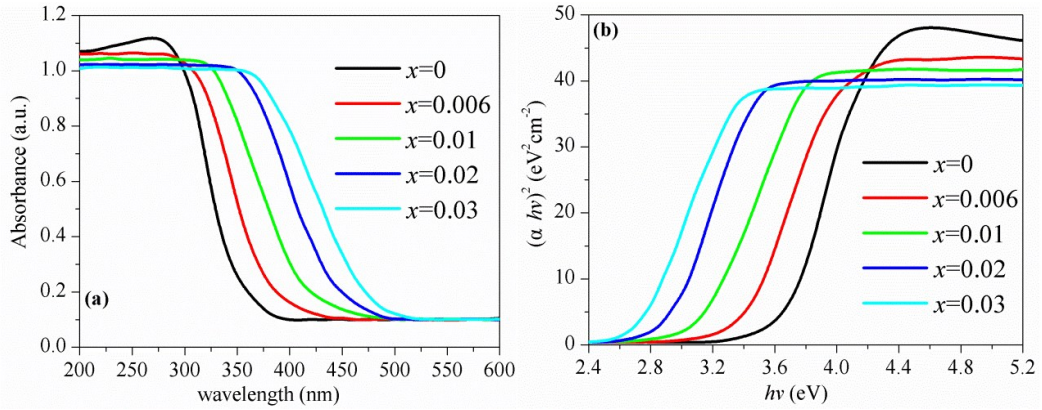

Fig. 5 (a) Optical absorption spectra and (b) Tauc's plot for the band gap values for $Zn_{(1-1.5x)}Fe_xS$ photocatalysts.

RSC Advances Accepted Manuscript

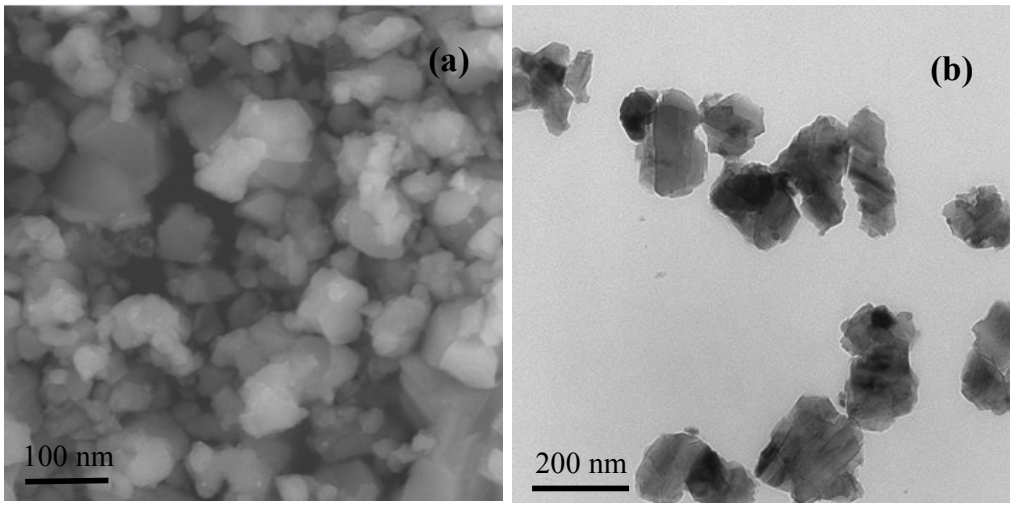

Fig. 6 (a) SEM and (b) TEM images of the $Zn_{0.97}Fe_{0.02}S$ photocatalysts.

RSC Advances Accepted Manuscript

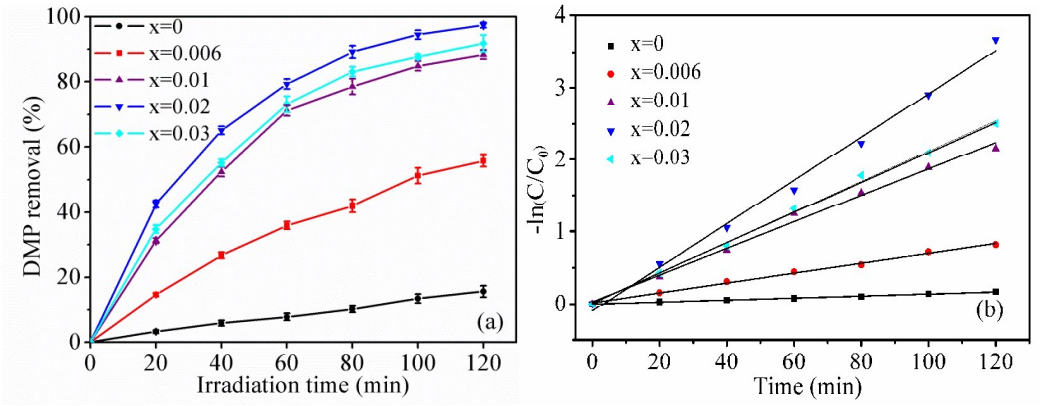

Fig. 7 Photocatalytic degradation of DMP in the presence of undoped and Fe-doped ZnS under visible light (inset shows its ln C_0/C vs. time graph).

RSC Advances Accepted Manuscript